3D mechanical measurements with an atomic force microscope on 1D structures.

Kallesøe, Christian; Larsen, Martin Benjamin Barbour Spanget; Bøggild, Peter; Mølhave, Kristian

Published in:
Review of Scientific Instruments

Link to article, DOI:
10.1063/1.3681784

Publication date:
2012

Document Version
Publisher's PDF, also known as Version of record

AIP | Review of Scientific Instruments

3D mechanical measurements with an atomic force microscope on 1D structures

Christian Kallesøe, Martin B. Larsen, Peter Bøggild, and Kristian Mølhave

Citation: Rev. Sci. Instrum. **83**, 023704 (2012); doi: 10.1063/1.3681784
View online: http://dx.doi.org/10.1063/1.3681784
View Table of Contents: http://rsi.aip.org/resource/1/RSINAK/v83/i2
Published by the American Institute of Physics.

3D mechanical measurements with an atomic force microscope on 1D structures

Christian Kallesøe,[a),b)] Martin B. Larsen, Peter Bøggild, and Kristian Mølhave[b)]
Department of Micro- and Nanotechnology, Technical University of Denmark, Kgs. Lyngby, DK-2800, Denmark

(Received 15 October 2010; accepted 13 January 2012; published online 9 February 2012)

We have developed a simple method to characterize the mechanical properties of three dimensional nanostructures, such as nanorods standing up from a substrate. With an atomic force microscope the cantilever probe is used to deflect a horizontally aligned nanorod at different positions along the nanorod, using the apex of the cantilever itself rather than the tip normally used for probing surfaces. This enables accurate determination of nanostructures' spring constant. From these measurements, Young's modulus is found on many individual nanorods with different geometrical and material structures in a short time. Based on this method Young's modulus of carbon nanofibers and epitaxial grown III-V nanowires has been determined. © *2012 American Institute of Physics*. [doi:10.1063/1.3681784]

I. INTRODUCTION

The mechanical strength and rigidity of nanostructures such as nanowires and carbon nanotubes (CNTs) are important properties for a range of applications, including CNT-AFM tips,[1,2] composite materials,[3–5] resonators,[6–9] and relays.[10–12] Important factors which have great influence on the mechanical properties of nanostructures are surfaces states and defects affecting Young's modulus of the wires,[13] heterostructure interfaces, and the epitaxial interface between wire and substrate. For multiwalled and singlewalled CNTs, several techniques on measuring Young's Modulus have been established.[13–17] For example, a scanning electron microscope (SEM) equipped with manipulation stages,[14] scanning tunneling microscope (STM)[15] and atomic force microscopes (AFM)[13,16,17] setups have been employed to measure plastic and elastic deformation parameters of CNTs. San Paulo *et al*. reported on AFM mechanical measurements on both single and double clamped silicon nanowires grown by the vapor-liquid-solid (VLS) mechanism.[18] Furthermore, vibration analysis has been successfully used to measure the mechanical properties of CNTs *in situ* TEM.[19,20] However, not many experimental tests on mechanical properties have been performed for III-V nanowires, and a simple standard equipment method for 3D mechanical characterization has been missing, that can be used on e.g., nanowires standing up from a substrate.

In this work, we have developed a simple method to characterize the mechanical properties of nanostructures such as nanowires and tubes. With an atomic force microscope (AFM) the cantilever probe is used to deflect a horizontally aligned nanorod at different positions along the nanorod, which enables accurate determination of the spring constant, see Fig. 1. The mechanical properties are measured in 3D with nanoscale resolution along the nanowire, while the exact spatial and force resolution is determined by the AFM. Characterizing a single nanowire as in Ref. 13 can provide measurements of its mechanical properties, but the presented method allows measurement of the mechanical properties as the wire stands attached to its substrate as needed for any nanomechanical use of the nanostructure, where the clamping influence will be essential. Furthermore, the method can be used to map out individual nanostructures in many other geometries than Ref. 13, requiring a verification of the structures dimensions. From this, Young's modulus of carbon nanofibers (CNFs) and epitaxial grown III-V nanowires has been determined. The method can find applications also in the new *in situ* SEM and TEM force sensing systems, such as the nanofactory AFM system.

II. ATOMIC FORCE MICROSCOPE SETUP

In this work, an AFM is used to directly measure the force-distance (FD) characteristics at varying distance from the substrate. During this process, the nanowires remain in their as-grown position, as illustrated in Fig. 1(a). The upper surface of the cantilever is used to deflect the nanowire at different positions along the nanowire, thus allowing for mapping of the mechanical properties in 3D with nanoscale resolution along the nanowire. The flat apex provides a well defined contact geometry, whereas the tip itself often has several facets at different angles. The substrate can be moved with nanoscale resolution and the deflection of the AFM cantilever was measured using photodiodes creating a A-B voltage signal (Fig. 1(a)). We estimate a 1 nm resolution of the stage.

The AFM used for the experiments was of type Veeco CPII and data was collected using Veeco Data Acquisition in connection with a free "AUTOHOTKEY" control software program[21] controlling the *x* and *y* position of the stage and automating the data acquisition process. Each sample substrate was attached by carbon tape to a PMMA block, situated on a magnetic base plate, thus the substrate surface was perpendicular to the base plate. Both sample and cantilever were grounded in order to avoid electrical fields between them,

[a)] Present address: Centre for Microtechnology and Surface Analysis, Danish Technical Institute, Taastrup, DK-2630, Denmark.
[b)] Authors to whom correspondence should be addressed. Electronic mail: chkl@teknologisk.dk and kristian.molhave@nanotech.dtu.dk.

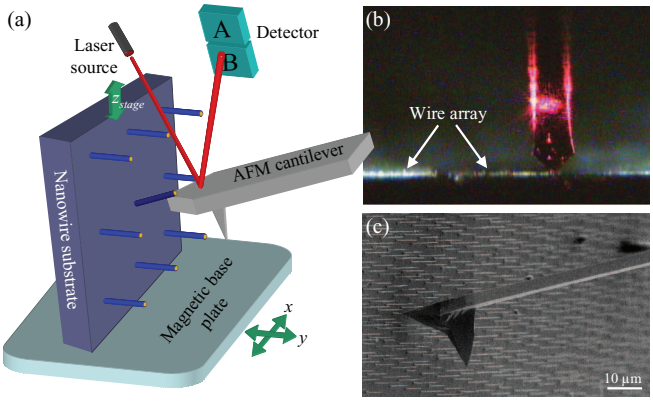

FIG. 1. (Color online) (a) Schematic of the measuring setup. (b) Optical microscope view in the AFM. The Veeco CPII AFM has a built in optical microscope with high resolution. Individual nanowires scatter light very efficiently and makes it possible to locate them. Nanowires are identified as small white rods scattering the light as indicated by the arrow. Alignment of the cantilever using the optical microscope is, as the image indicates, insufficient and is therefore done using the A-B signal thus testing a possible contact. (c) To verify the nanowire bending behavior, *in situ* experiments in SEM were performed using a Smaract nanomanipulator. These experiments, however, do not provide any force measurements.

which were found to be strongly disturbing the measurements by either attraction or repulsion. For the substrate, this was done by using copper tape, to gain a connection to the base plate. The vertical position of the stage (with the nanowire), z_{stage}, can be controlled and measured mechanically by the AFM using a standard function of the AFM called the force-distance curve (FD) (having a z_{stage} range of 8 μm). Thus, the stage was moved downwards while measuring the cantilever deflection, z_{cl}, from the laser A-B diode signal (Fig. 2(a)). The CPII has a built in optical microscope with high resolution. Individual nanowires scatter light very efficiently thus making it possible to locate them. The x position of the substrate was optimized so that the cantilever only contacts one nanowire. The number of contacted nanowires can be read out from the FD curves as multiple individual nanowires will show abnormalities in the peaks in the FD curve, as shown in Fig. 4(c).

III. PURE BENDING OF A POINT LOADED NANOWIRE

Regarding the nanowire as a circular beam, fixed at one end and free at the other, see Fig. 2(a), the bending of the beam can be found for a point loaded beam,[22]

$$\frac{d^2 z_{nw}(y)}{dy^2} = \frac{M(y)}{EI} = \frac{F}{EI}(L - y), \tag{1}$$

where M is the applied moment at position y given by $M = -F(L - y)$ and F is the point force at position L. It is derived from the Euler-Bernoulli equation for the case of small deflection ($z_{stage}/L < 10\%$). Thus, a small deflection is assumed, i.e., a limit on the cantilever-nanorod angle of about 5° which also include any initial angle between them. This, as will be shown later, is fulfilled as the nanowire slips off the cantilever before large deflections are achieved. The equation is fixed by the boundary conditions $dz_{nw}/dy\,|_{y=0} = 0$ and $z_{nw}(0) = 0$, as both angle and deflection at the root of the wire are zero.

A linear tapering of the wire will cause the bending stiffness $EI(y)$ to vary as function of y. The area moment of inertia is given by

$$I(y) = \frac{\pi D(y)^4}{64} = \frac{\pi}{64}\left(D_r - y\frac{D_r - D(L)}{L}\right)^4, \tag{2}$$

where D_r is the diameter at the root of the wire and $D(L)$ is the diameter at the point load $y = L$. The angle, dz/dy, can found by integrating Eq. (1) and further integration results in the deflection which at the point load $y = L$ is given by

$$z_{nw}(L) = \int_0^L \int_0^L \frac{F(L-y)}{E\frac{\pi}{64}\left(D_r - y\frac{D_r - D(L)}{L}\right)^4} dy dy$$

$$= \frac{64FL^3}{3\pi E D_r^3 D(L)}, \tag{3}$$

resulting in the spring constant

$$k_{tap}(L) = \frac{3\pi E D_r^3 D(L)}{64L^3}. \tag{4}$$

The mechanical properties of the nanorods are calculated from the set of FD curves measured with the AFM. The spring constant of the nanowire will increase as the AFM contact point on the nanowire approaches the nanowire substrate, thus increasing the slope of the FD curves, $\alpha(y)$, see Figs. 2(b)

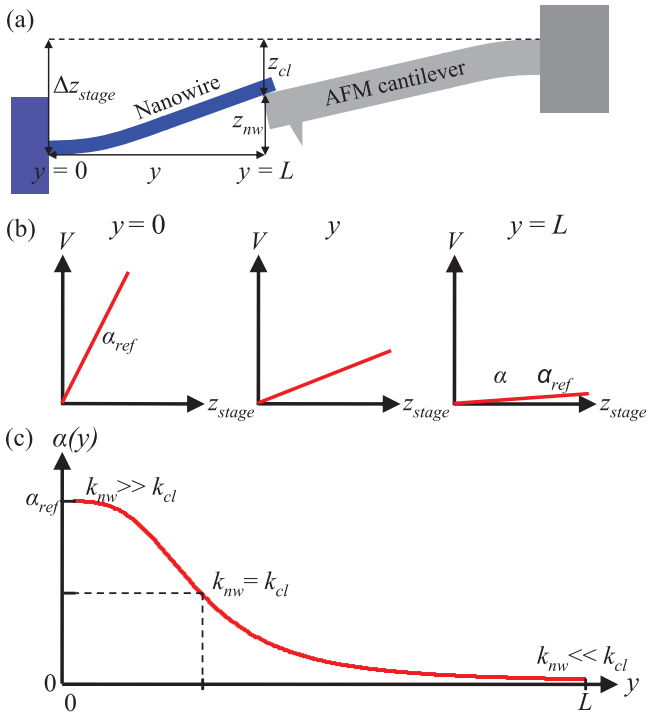

FIG. 2. (Color online) Illustration of the nanowire-cantilever measurement method and the FD curves as function of y. (a) The nanowire is regarded as a circular beam, fixed at one end and free at the other. The bending of the nanowire can be found from the nanowire stage position and cantilever deflection measured from the A-B diode FD curves. (b) As the cantilever approaches the nanowire substrate, the nanowire spring constant increases causing a stronger cantilever bending, thus the slope of the FD curve will increase. (c) A representative plot of the slopes of the FD curves, $\alpha(y)$, as a function of y. These plots are fitted to Eq. (11) to obtain the mechanical properties of the nanorods.

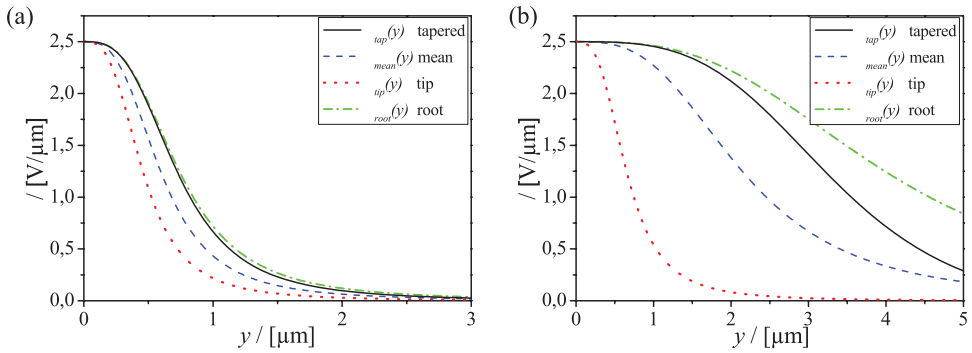

FIG. 3. (Color online) Plots of $\alpha(y)$ for two nanorods having dimensions comparable with the measured samples presented later on, showing the importance of the tapered model. (a) Wire with $D_r = 100$ nm, $D_t = 70$ nm, and $L = 3$ μm. (b) Wire with $D_r = 350$ nm, $D_t = 90$ nm, and $L = 5$ μm. The three untapered curves are calculated using the mean diameter (dashed), the tip diameter (dotted), and the root diameter (dash-dotted) in order to compare with the linear tapered wire having a y dependent diameter (full). All curves in both graphs are calculated for $E = 85.9$ GPa, Young's modulus of bulk GaAs.

and 2(c). Both the stage position change, Δz_{stage}, and the cantilever deflection, z_{cl}, are measured by the AFM, mechanically and optically, respectively, and from these the nanowire deflection can be found, see Fig. 2(a),

$$z_{nw} = \Delta z_{stage} - z_{cl}. \tag{5}$$

The resulting forces are opposite and equal,

$$0 = \mathbf{F}_{cl} + \mathbf{F}_{nw}. \tag{6}$$

Projecting them onto the z axis and using Hooke's law results in

$$0 = k_{cl} z_{cl} - k_{nw} z_{nw}, \tag{7}$$

and using Eqs. (5) and (7) the spring constant of the nanowire can be expressed as

$$k_{nw} = \frac{k_{cl} z_{cl}}{\Delta z_{stage} - \Delta z_{cl}}. \tag{8}$$

z_{cl} is found from the A-B diode voltage, ΔV, measured by the AFM. It is given by the linear relationship $z_{cl} = \alpha_{ref} \Delta V$, where α_{ref} is the reference response, i.e., a measurement of the cantilever deflection when the cantilever is pressed against a solid substrate (where $z_{cl} = \Delta z_{stage}$). Furthermore, the relationship between ΔV and Δz_{stage} can be expressed by using a variable, $\alpha(y)$. Thus, the following two expressions are given

$$\alpha_{ref} = \frac{\Delta V}{z_{cl}}, \quad \alpha(y) = \frac{\Delta V}{\Delta z_{stage}}, \tag{9}$$

The spring constant can then be rewritten as

$$k_{nw} = \frac{k_{cl}}{\frac{\alpha_{ref}}{\alpha(y)} - 1}. \tag{10}$$

Isolating for $\alpha(y)$ and inserting the spring constant for a tapered wire (Eq. (4)) with a point load at y then gives the relation, which can be fitted to the measurements

$$\alpha(y) = \frac{\alpha_{ref}}{\frac{64 k_{cl}}{3\pi D_r^3 D(y) E} y^3 + 1}. \tag{11}$$

From the cantilever manufacturer the cantilever spring constant is known as $k_{cl} = 3$ N/m and the resonant frequency is 75 ± 15 kHz indicating an uncertainty of the spring constant of ± 1.2 N/m. The reference slope α_{ref} was measured by pressing the cantilever against a solid substrate, thus $\Delta z_{stage} = z_{cl}$. This was done for every cantilever used, with a value of $\alpha_{ref} = 2.5$ V/μm. The FD curves are measured at different y positions along the nanowire, using an automated autohotkey script developed for these measurements. The AUTOHOTKEY program measures the FD curve, logs the y position along with the FD data, and then adds a small predefined value to the y position. The program then repeats these steps until the substrate and cantilever come in contact. To find Young's modulus, $\alpha(y)$ is plotted as function of y, as illustrated in Fig. 2,

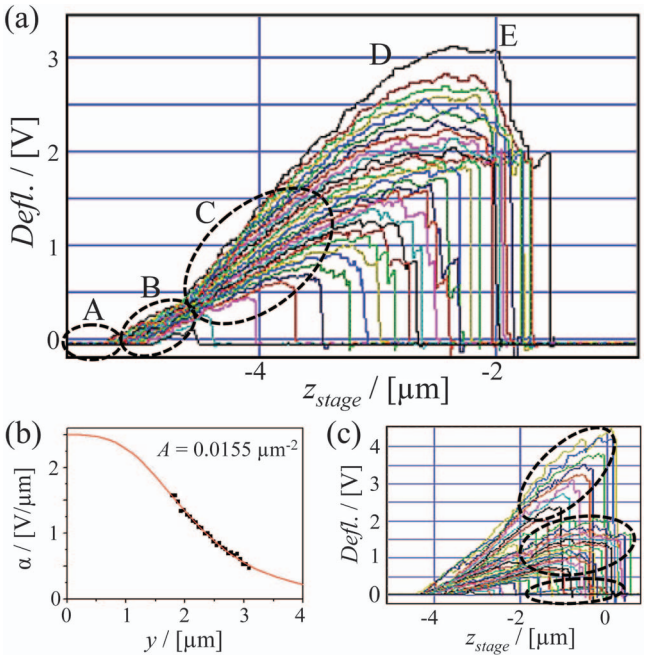

FIG. 4. (Color online) Example of FD curve measurements on a CNF with $D_r = 190$ nm, $D_t = 120$ nm, and $L = 3$ μm. The different colors of the curves in (a) indicates different measurements on the CNF at various y positions plotted in the same graph, with the stage position on the horizontal axis and the cantilever deflection on the vertical axis. The entire plot of the FD curves for the CNF is shown and the various regions are indicated (and explained in Fig. 5). From region "A" the noise can be found and in "B" the constant slopes are seen. In region "C", a representative window is chosen for the slope calculations. (b) $\alpha(y)$ from region "C" is plotted and fitted to Eq. (12). (c) Example of a complex multi-nanowire bundle giving a more complex signal. Three different region "D"s can be identified (indicated by the dashed circles), revealing three different nanowires.

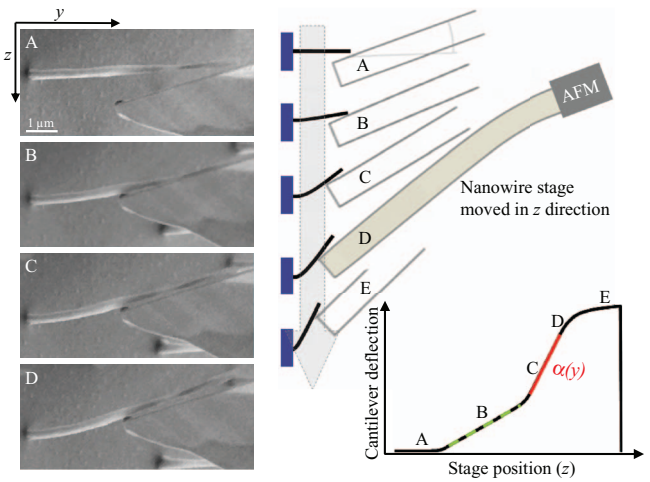

FIG. 5. (Color online) SEM images and illustration of the mechanism behind the FD behavior. The *in situ* SEM experiments were performed on a CNF array using a Smaract nanomanipulator, where the CNF sample is moved upwards toward the cantilever. "A" The fiber and cantilever are brought into contact. The cantilever will always make first contact to the apex of the fiber, due to the difference in angle. "B" As the fiber moves downwards, it becomes parallel with the cantilever. "C" The interaction between fiber and cantilever is now y-dependent and the slope of the curve in this region, $\alpha(y)$, is used for the calculations. "D" and "E" When the fiber is moved further down, it slips in small steps along the cantilever before it finally slides off the cantilever.

and fitted to

$$\alpha(y) = \frac{\alpha_{ref}}{\frac{A}{D(y)}(y - y_0)^3 + 1}, \tag{12}$$

which corresponds to Eq. (11) where α_{ref} is known from the reference measurement and y_0 is the wire root position. The interesting value is A,

$$A = \frac{64 k_{cl}}{3\pi D_r^3 E}, \tag{13}$$

from which Young's modulus can be found. $D(y)$ is dependent on the load position, with the relation $D(y) = D_r - T \cdot y$, where T is the tapering slope of wire, i.e., $T = (D_r - D_t)/L$, and D_t is the diameter at the tip of the wire.

To demonstrate the impact of the wire tapering on the mechanical properties, Fig. 3 shows $\alpha(y)$ for nanorods having dimensions comparable with the later on presented samples. Included are plots for both tapered rods and untapered rods with $D(y) = D_r$ (root diameter), $D(y) = D_t$ (tip diameter), and $D(y) = (D_r + D_t)/2$ (mean diameter). Two graphs are presented: Fig. 3(a) shows $\alpha(y)$ for a wire with $D_r = 100$ nm, $D_t = 70$ nm and $L = 3\mu$m (the GaAs wire array dimensions presented in Sec. V A) and Fig. 3(b) shows $\alpha(y)$ for a tube with stronger tapering having $D_r = 350$ nm, $D_t = 90$ nm and $L = 5$ μm (the CNF array dimensions presented in Sec. V B).

IV. QUALITATIVE MODEL OF THE SIGNAL

An example of a measurement series is given in Fig. 4 showing FD curves for varying y positions. Several different regions are recognized, with only noise measured in region "A", all slopes being equal in region "B" (though a minor variation may be observed due to relative motion of the nanorod tip on the cantilever) and with a y dependent slope in region "C". The FD curve contains several regions that correspond to specific contact regimes between the cantilever and nanorod. The minimum deflection and force that can be detected is determined by the amount of noise measured by the A-B diode signal in region "A". From Fig. 4 $\Delta V_{noise} = 0.01$ V, corresponding to a deflection of $z_{min} = \Delta V_{noise}/\alpha_{ref} = 4$ nm. Using Hooke's law the noise floor of the force detection is then: $F_{min} = k_{cl} z_{min} = 12$ nN. A LabView program has been developed to calculate $\alpha(y)$ as function of the y-position within a representing window, region "C". In Fig. 4(b), $\alpha(y)$ is plotted as a function of y and fitted to Eq. (12). Precise measurements of the wire dimensions are needed in order to achieve an accurate determination of the structural stiffness and Young's modulus (using Eq. (13)); however, only the relative y-positions need to be known, as the exact root position (the y zero point) is not required but instead obtained from the fitting.

To understand the typical FD curve, the experiment was repeated inside a SEM using a Smaract nanomanipulator for detailed investigation of the cantilever-nanorod mechanical contact, without reading out the force, as shown in Fig. 5. The cantilever was tilted with respect to a CNF substrate as in the AFM measurements, thus the contact to the cantilever was established at the fiber tip when moving the CNF substrate downwards towards the cantilever, represented as "A" in Fig. 5. Moving the CNF sample further down, the cantilever exerted a force as a point load at the tip of the fiber, until the fiber and cantilever were parallel, region "B". Therefore, the slope of the FD curve in this region will be independent of the y stage position. Moving the fiber further up, resulted in the cantilever acting as a point load at a y dependent position on the fiber, region "C" as the fiber pivots around the AFM edge, thus the slope of the FD curve in "C" will be y dependent. At some point the fiber started to slip in small steps along the cantilever before it finally slided sideways off the cantilever due to the triangular shape of the cantilever, region "D". As a result, the slope of this part of the FD curve will decrease, where nonlinear effects due to detector saturation also can contribute. The fiber was observed in SEM to slide sideways off the cantilever, due to the triangular shape of the cantilever, and the A-B signal will thus drop to zero in region E as contact is lost. Comparing to Fig. 4, the different regions

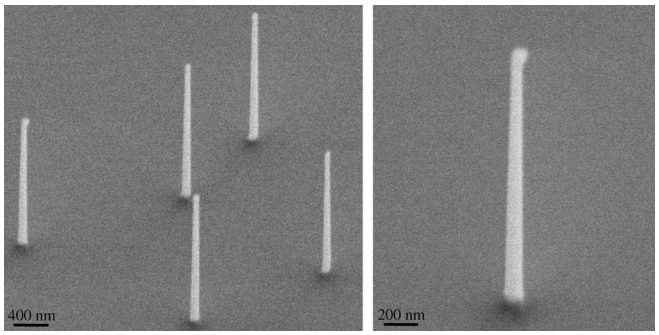

FIG. 6. SEM images of the measured GaAs nanowire array. The wires are slightly tapered with little dimension variation. Root diameter: $D_r = 99 \pm 1$ nm, tip diameter: $D_t = 68 \pm 1$ nm, and length: $L = 3 \pm 0.2$ μm.

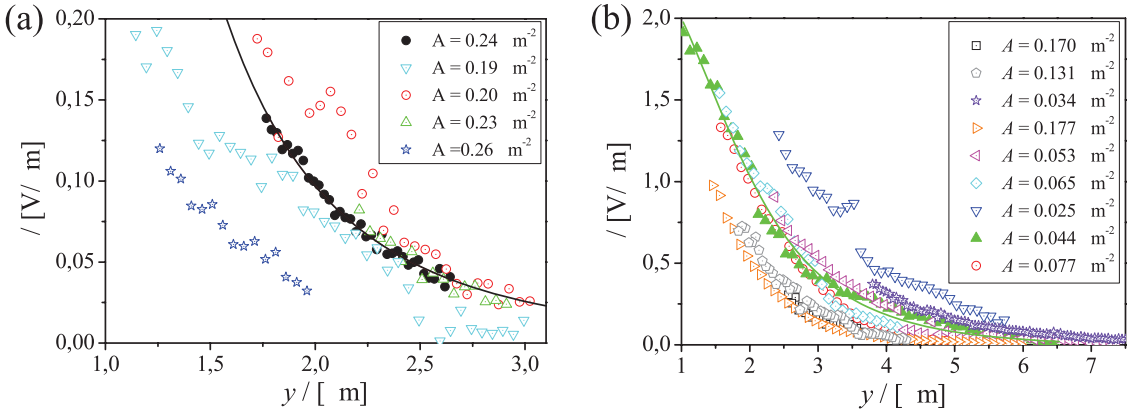

FIG. 7. (Color online) Measured $\alpha(y)$ for GaAs nanowires (a) and CNFs (b). The small $\alpha(y)$ values for the GaAs nanowires indicates a small bending stiffness of the wires compared to the fibers. The small bending stiffness of the wires can be ascribed to their small diameter and a low Young's modulus. The black (a) and green (b) lines are examples of fitted curves from (12).

are clearly seen in the inserts labeled A, B, C, and D, and we hence have a qualitative model of the overall FD curve shape with the y-dependent part in region "C".

V. MECHANICAL MEASUREMENT RESULTS

In Secs. V A and V B, measurements of GaAs nanowires grown on GaAs(111) and Carbon nanofibers (CNF) grown on SiO_2 are presented.

A. Mechanical properties of GaAs nanowires

Figure 6 shows SEM images of the measured GaAs nanowires. The wires are slightly tapered with little dimension variation. The root diameter is measured to be $D_r = 99 \pm 1$ nm and the tip diameter is $D_t = 68 \pm 1$ nm. The length of the wires is $L = 3.0 \pm 0.2$ μm. Using Eq. (13), Young's modulus can be found from the fitted A values in Fig. 7(a) from the following measurements:

$$E_{nw} = \frac{64k_{cl}}{3\pi D_r^3 A} = \frac{20.8 \pm 8.5\text{GPa}}{A \cdot \mu\text{m}^2}, \tag{14}$$

where the uncertainty includes both the nanowire dimension and AFM cantilever uncertainties. From Eq. (4), the spring constant as a function of wire length is given by

$$k_{tap}(y) = \frac{3\pi E D_r^3 D(y)}{64y^3}. \tag{15}$$

All results on GaAs nanowires are presented in Table I (including standard deviations (σ)) and Fig. 7(a).

The large standard deviations for E seen in Table I stem mainly from the uncalibrated AFM cantilever. A calibrated cantilever would reduce the uncertainty to 10%. The mean value of Young's modulus is estimated to $\bar{E} = 94.1$ GPa, comparable to a bulk value of $E_{bulk} = 85.9$ GPa.[23] A mean spring constant at the end of the wire ($L = 3$ μm) is calculated to $\bar{k}_{nw} = 0.034$ N/m.

B. Mechanical properties of carbon nanofibers

Figure 8 shows SEM images of the measured CNFs. A strong tapering is seen with $D_r = 350 \pm 30$ nm and $D_t = 90 \pm 40$ nm, with a very big spread in both diameter and length. The length of the fibers is $L = 5.9 \pm 1.0$ μm. Furthermore, the tapering is seen not to be linear, and some of the fibers are with two tips, thus the results are with a large uncertainty. Young's modulus can be found from the fitted A in Fig. 7(b),

$$E_{cnf} = \frac{64k_{cl}}{3\pi D_r^3 A} = \frac{0.48 \pm 0.23\text{GPa}}{A \cdot \mu\text{m}^2}. \tag{16}$$

Tapered results on the CNFs are presented in Table II and Fig. 7(b). The mean value of the bending modulus of the tapered structures is estimated to $\bar{E}_{tap} = 8.4$ GPa, with a very large uncertainty due to both uncalibrated AFM cantilever and the large spread in radius and shape of the fibers. A mean spring constant at the end of the tapered fibers ($L = 5$ μm) is calculated to be $\bar{k}_{nw} = 0.04$ N/m.

VI. DISCUSSION

A qualitative model has been made for the overall FD signal describing the region of interest (region "C") for

TABLE I. GaAs nanowires mechanical measurements.

$A/[\mu\text{m}^{-2}]$	$\sigma_A/[\mu\text{m}^{-2}]$	E/[GPa]	σ_E/[GPa]	$k_{tap}(y)$
0.24	0.02	86.7	42.7	$(1.23\ \mu\text{m} - 0.124y)\ \mu\text{m}^2 \cdot y^{-3}$ N/m
0.19	0.006	109.5	48.2	$(1.55\ \mu\text{m} - 0.156y)\ \mu\text{m}^2 \cdot y^{-3}$ N/m
0.20	0.06	104.0	77.6	$(1.48\ \mu\text{m} - 0.149y)\ \mu\text{m}^2 \cdot y^{-3}$ N/m
0.23	0.07	90.4	64.5	$(1.28\ \mu\text{m} - 0.129y)\ \mu\text{m}^2 \cdot y^{-3}$ N/m
0.26	0.005	80.0	34.2	$(1.13\ \mu\text{m} - 0.114y)\ \mu\text{m}^2 \cdot y^{-3}$ N/m

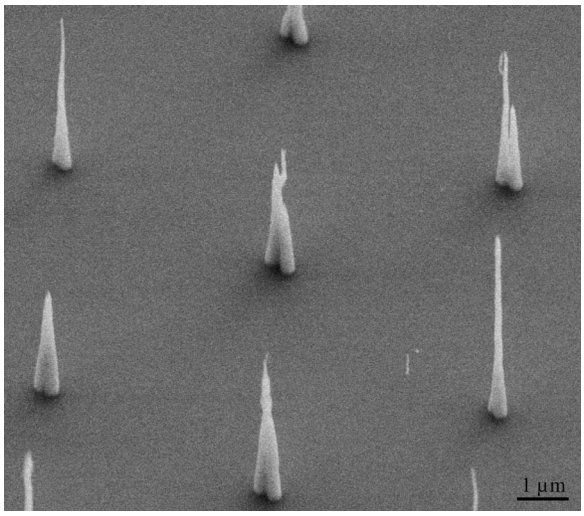

FIG. 8. SEM image of the measured CNF array, with a strong tapering structure and a large dimension variation.

mechanical measurements. As mentioned previously, the minimum deflection and force that can be detected using the proposed method is determined by the AFM, i.e., the amount of noise measured by the A-B diode signal resulting in a minimum detectable force of $F_{min} = k_{cl} z_{min} = 12$ nN. Reducing the noise is therefore essential for the measurement of very thin nanowires. The triangular shape of the cantilever eases the contact procedure where only one wire should be contacted. However, the method is not capable of contacting individual nanowires if the wire-wire distance becomes smaller than the length of the wires. The fact that the mechanical properties are measured along the nanowire length, means that the method is suitable for a mechanical mapping of structures with varying material composition (heterostructures) or morphology (e.g., narrowing sections), measuring from the tip of the nanowire to determine the y-position. This requires a verification of the structures dimensions.

The z range of the cantilever is not decreased as the cantilever approaches the substrate. Due to the triangular shape of the cantilever tip, the wire can, however, slide off sideways, thus region "E" in Fig. 5 is seldom reached. However, a measurement will still result in the wire breaking off as the point load approaches the substrate and the applied moment at the nanowire root will exceed the ultimate strength of the nanowire material. Thus, an $\alpha(y)$ value of 2.5 is never reached as also seen in Fig. 7. Gradual decrease in z range along the wire would improve this.

The GaAs nanowires having diameter of less than 100 nm, are seen to have a Young's modulus of 94 GPa which agree well with the bulk value of 85.9 GPa. The small discrepancy between the estimated and bulk values of Young's modulus can be attributed to measurement uncertainties of the nanowire dimensions, but especially a systematic error from the spring constant of the cantilever. A calibrated cantilever should be used in the future. The agreement between bulk and measured wire modulus values stems with what have previously been reported by San Paulo *et al*. where a Young's modulus of 186 GPa were measured for Si wires with diameters below 100 nm, comparable to a bulk value of 169 GPa for Si(111).[18]

CNTs are known for their incredible stiffness with Young's modulus in the order of 100–1000 GPa.[16,19,20] The low Young's modulus found for the carbon nanofibers here using the tapered fitting, indicates that no strong tubular carbon structure is present. The scatter in the data for the CNFs can be explained by the fact that the measured bending stiffness is dominated by the physical dimensions of the fiber and is not a reflection of the model itself.

VII. CONCLUSION

We have established a method which enables mechanical measurements on 3D nanostructures such as individual epitaxially grown nanowires on their substrates, without any preparation steps, such as moving nanowires to other surfaces. The mechanical properties were measured with nanometer resolution along the nanowires determined by the AFM, and a force resolution of 12 nN. From these measurements Young's moduli were found on many individual GaAs nanowires and carbon nanofibers, also taking their tapering structure into account. For the GaAs nanowires having diameter of less than 100 nm, a Young's modulus in the order of 94 GPa were estimated, larger than the bulk value of 85.9 GPa. This increase was ascribed to a systematic error stemming from the cantilever spring constant. Increased precision would require determination of the exact cantilever spring constant.

Using arrays with much smaller densities would allow for a previous determination of the exact wire dimensions in SEM

TABLE II. CNFs mechanical measurements.

$A/[\mu\text{m}^{-2}]$	$\sigma_A/[\mu\text{m}^{-2}]$	E/[GPa]	σ_E/[GPa]	$k_{tap}(y)$
0.170	0.032	2.8	1.9	$(6.2\ \mu\text{m} - 0.9y)\ \mu\text{m}^2 \cdot y^{-3}$ N/m
0.131	0.014	3.7	2.2	$(8.1\ \mu\text{m} - 1.0y)\ \mu\text{m}^2 \cdot y^{-3}$ N/m
0.034	0.0004	14.1	6.9	$(31\ \mu\text{m} - 3.9y)\ \mu\text{m}^2 \cdot y^{-3}$ N/m
0.177	0.008	2.7	1.4	$(5.9\ \mu\text{m} - 0.8y)\ \mu\text{m}^2 \cdot y^{-3}$ N/m
0.053	0.007	9.1	5.6	$(20\ \mu\text{m} - 2.5y)\ \mu\text{m}^2 \cdot y^{-3}$ N/m
0.065	0.009	7.4	4.6	$(16\ \mu\text{m} - 2.1y)\ \mu\text{m}^2 \cdot y^{-3}$ N/m
0.025	0.002	19.2	10.7	$(42\ \mu\text{m} - 5.4y)\ \mu\text{m}^2 \cdot y^{-3}$ N/m
0.044	0.005	10.9	6.5	$(24\ \mu\text{m} - 3.1y)\ \mu\text{m}^2 \cdot y^{-3}$ N/m
0.077	0.008	6.2	3.6	$(14\ \mu\text{m} - 1.8y)\ \mu\text{m}^2 \cdot y^{-3}$ N/m

and optical location of individual nanowires with known dimensions. SEM or TEM combined with a piezoelectric stage moving a cantilever, would provide *in situ* mechanical measurements thus also revealing the transition between elastic behavior and brittle breakage of the wire.

The method opens up for mapping of the varying mechanical properties along, e.g., heterostructures, such as GaAs-GaP nanowires, or with varying diameters. Furthermore *in situ* experiments with force readout using, e.g., piezoresistive AFM probes would be useful for a perfect correlation of both nanorod dimension and the FD curves.

ACKNOWLEDGMENTS

We thank Ken Teo, Thomas Mårtensson, Monica Lexholm, and Lars Samuelson for providing samples and acknowledge financial support of the Danish Agency for Science, Technology and Innovation through grant No. 26-04-0258. Furthermore, we thank Matthias Goldschmidt and Lau Carlsen for experimental assistance.

[1]H. Nishijima, S. Kamo, S. Akita, Y. Nakayama, K. I. Hohmura, S. H. Yoshimura, and K. Takeyasu, Appl. Phys. Lett. **74**, 4061 (1999).
[2]K. Carlson, K. N. Andersen, V. Eichhorn, D. H. Petersen, K. Mølhave, I. Y. Y. Bu, K. B. K. Teo, W. I. Milne, S. Fatikow, and P. Bøggild, Nanotechnology **18**, 345501 (2007).
[3]P. X. Gao, J. Song, J. Liu, and Z. L. Wang, Adv. Mater. **19**, 67 (2007).
[4]R. Andrews, D. Jacques, A. M. Rao, T. Rantell, F. Derbyshire, Y. Chen, J. Chen, and R. C. Haddon, Appl. Phys. Lett. **75**, 1329 (1999).
[5]P. J. F. Harris, E. Hernández, and B. I. Yakobson, Am. J. Phys. **72**, 415 (2004).
[6]A. San Paulo, N. Arellano, J. A. Plaza, R. He, C. Carraro, R. Maboudian, R. T. Howe, J. Bokor, and P. Yang, Nano Lett. **7**, 1100 (2007).
[7]C. Li and T. W. Chou, Phys. Rev. B **68**, 73405 (2003).
[8]C. Li and T. W. Chou, Appl. Phys. Lett. **84**, 5246 (2004).
[9]C. Li and T. W. Chou, Appl. Phys. Lett. **84**, 121 (2004).
[10]K. Terabe, T. Hasegawa, T. Nakayama, and M. Aono, Nature (London) **433**, 47 (2005).
[11]S. W. Lee, D. S. Lee, R. E. Morjan, S. H. Jhang, M. Sveningsson, O. A. Nerushev, Y. W. Park, and E. E. B. Campbell, Nano Lett. **4**, 2027 (2004).
[12]R. H. Baughman, A. A. Zakhidov, and W. A. de Heer, Science **297**, 787 (2002).
[13]E. W. Wong, P. E. Sheehan, and C. M. Lieber, Science **277**, 1971 (1997).
[14]M. F. Yu, O. Lourie, M. J. Dyer, K. Moloni, T. F. Kelly, and R. S. Ruoff, Science **287**, 637 (2000).
[15]M. S. Wang, J. Y. Wang, Q. Chen, and L. M. Peng, Adv. Funct. Mater. **15**, 1825 (2005).
[16]J. P. Salvetat, G. A.D. Briggs, J. M. Bonard, R. R. Bacsa, A. J. Kulik, T. Stöckli, N. A. Burnham, and L. Forró, Phys. Rev. Lett. **82**, 944 (1999).
[17]J. Song, X. Wang, E. Riedo, and Z. L. Wang, Nano Lett. **5**, 1954 (2005).
[18]A. San Paulo, J. Bokor, R. T. Howe, R. He, P. Yang, D. Gao, C. Carraro, and R. Maboudian, Appl. Phys. Lett. **87**, 053111 (2005).
[19]M. M. J. Treacy, T. W. Ebbesen, and J. M. Gibson, Nature (London) **381**, 678 (1996).
[20]P. Poncharal, Z. L. Wang, D. Ugarte, and W. A. de Heer, Science **283**, 1513 (1999).
[21]See http://www.autohotkey.com/ for control software program: Script for AUTOHOTKEY - Free Mouse and Keyboard Macro Program with Hotkeys and AutoText.
[22]R. J. Roark and W. C. Young, *Roark's Formulas for Stress and Strain* (McGraw-Hill, New York, 1989).
[23]See http://www.ioffe.rssi.ru/SVA/NSM/Semicond/ for semiconductors on NSM, Ioffe Physico-Technical Institute.